ELSEVIER

Acta MATERIALIA

Application of single pan thermal analysis to Cu–Sn peritectic alloys

F. Kohler, T. Campanella [1], S. Nakanishi [2], M. Rappaz *

Computational Materials Laboratory, Ecole Polytechnique Fédérale de Lausanne, Station 12, CH-1015 Lausanne, Switzerland

Abstract

Single pan thermal analyses (SPTA) have been performed on Cu–14.5 wt.% Sn, Cu–21.3 wt.% Sn and Cu–26.8 wt.% Sn peritectic alloys. For this purpose, a SPTA assembly has been built and calibrated. As the latent heat is a function of temperature and composition during solidification of alloys, a new heat flow model coupled to a Cu–Sn thermodynamic database has been defined for the calculation of the corresponding evolutions of the solid mass fraction, $f_s(T)$. To verify the accuracy of this model, a close comparison with a micro-segregation model that includes back-diffusion in the primary α-solid phase has also been conducted successfully. The thermal analyses have finally shown that the Cu–Sn phase diagram recently assessed in the review of Liu et al. is the most reliable.
© 2007 Acta Materialia Inc. Published by Elsevier Ltd. All rights reserved.

Keywords: Thermal analysis; Peritectic solidification; Copper alloys; Thermodynamics

1. Introduction

Copper–tin peritectic alloys, also known as tin bronzes, are still widely used in many industrial applications. Due to their remarkable properties, i.e. high strength, high thermal conductivity, good wear resistance and machinability, these alloys are well adapted for the automotive and electronic industries. But, in spite of the commercial importance of Cu–Sn alloys, only a few studies have been made on their detailed solidification. Furthermore, the Cu–Sn phase diagram found in most metals handbooks is based on thermal analyses and metallographic observations performed before 1970 [1]. Only recently have the phase equilibria in the Cu-rich portion of the system been thoroughly reinvestigated by Liu et al. [2] using diffusion-couple, differential scanning calorimetry, high-temperature electron diffraction and high-temperature X-ray diffraction techniques. These

authors reassessed the Cu–Sn phase diagram for temperatures below the peritectic reaction $\alpha + \text{liquid} \rightarrow \beta$. In this review, two successive second-order ordering reactions from the β peritectic phase to the γ-phase were identified. Thus, rather than being a distinct phase, the γ-phase seems to be the DO3 ordered structure of the β-phase (see Section 4). Nevertheless, to the present authors' knowledge, the detailed solidification of Cu–Sn alloys for Sn compositions in the peritectic range has never been reported.

To measure the temperature of phase transformations in metals and alloys, differential thermal analysis (DTA) has been extensively used for many years [3–5]. DTA consists of analysing heat exchanges between a reference pan and a sample pan subjected to heating–cooling cycles. However, a major drawback of this method comes from its design and the sample size effect, as shown by Boettinger and Kattner [4] for pure metals and alloys. Due to the two-pan assembly and its relatively high thermal resistance, these authors reported that the latent heat was absorbed during melting or released during solidification over a wider temperature range, i.e. the so-called smearing effect. For pure metals, the latent heat typically appeared to be smeared over about 3 K [6]. Moreover, due to the relatively small size of the sample used in DTA, i.e. ∼20 mg, high

---
* Corresponding author. Tel.: +41 (0) 21693 2925; fax: +41 (0) 21693 5890.
  E-mail address: michel.rappaz@epfl.ch (M. Rappaz).
[1] Formerly at Rolex, Geneva, Switzerland.
[2] Master Student, Shibaura Institute of Technology, Tokyo 108-8548, Japan.

nucleation undercoolings are expected on cooling. Consequently, it is difficult to determine precisely the melting temperature for pure metals or the liquidus and solidus temperatures for alloys. For multicomponent alloys, Wu and Perepezko [5] developed an interrupted-heating DTA method to provide a more accurate determination of the liquidus temperatures.

In 2001, Dong and Hunt [7] proposed a novel single pan thermal scanning calorimeter (SPTSC), thereby introducing a new thermal analysis method named single pan thermal analysis (SPTA). Similar to the device used by Zou and Rappaz [8] for the solidification of grey cast iron, and unlike the conventional calorimeter used for DTA, the SPTSC consists of two imbricated crucibles. The sample to be studied is placed in the inner crucible and typically consists of a few grams of material. To perform a thermal analysis, this assembly is inserted in a furnace, its heating or cooling rate being precisely controlled. Heat exchanges between the sample and the surroundings are then measured by three thermocouples, i.e. one directly at the center of the sample and one in each crucible. In order to calibrate their SPTSC, Dong and Hunt [7] performed thermal analyses on a well-known material, i.e. reference material. Based on a simplified heat conservation equation in a volume, an appropriate relation was also derived to relate temperature and enthalpy changes. Dong and Hunt [7] used pure Al to check the accuracy of their method, and showed that the temperature variation during melting and solidification was very small. As a consequence, the smearing effect observed with DTA is not found with SPTA.

During the solidification of alloys, the enthalpy changes with composition and temperature [9]. In a recent paper, Dong et al. [10] have carried out SPTA on a Al–4.45 wt.% Cu alloy. Unlike most solidification models, which assume a constant latent heat, they showed that it was not possible to deduce the evolution of the solid mass fraction, i.e. $f_s(T)$, directly from enthalpy plots. Dong et al. rather used microsegregation models coupled to a thermodynamic database to get $f_s(T)$ indirectly from experimental enthalpy measurements [6,10].

In the present study, the same SPTA method has been applied to three compositions of the Cu–Sn peritectic system: Cu–14.5 wt.%Sn, Cu–21.3 wt.% Sn and Cu–26.8 wt.% Sn. Based on the SPTSC designed by Dong and Hunt [7], a SPTA assembly has been built and calibrated. In order to investigate the solidification of these alloys, a new heat flow model has been defined. Unlike most solidification models employed to date, temperature-dependent thermophysical properties have been used. Moreover, a coupling with a Cu–Sn ThermoCalc™ database has been performed in order to allow the use of time-dependent enthalpies. In order to assess the accuracy of the heat flow model, a close comparison with a microsegregation model that includes back-diffusion in the primary α-solid phase has been successfully conducted. The solidified microstructures have been observed by optical

microscopy and scanning electron microscopy (SEM). For a clear phase identification, concentration measurements have also been carried out using a microprobe. Finally, the observed solidification paths have been compared with the Cu–Sn phase diagram of Liu et al. [2].

2. Experimental method

The SPTA assembly consists of two imbricated crucibles, with a reduced thermal contact between them (insert in Fig. 1). For the outer envelope, a Ni crucible has been used, whereas the inner crucible containing the sample was made of boron nitride (BN). BN was used because of its rather good thermal conductivity and its non-wettability with most metals and alloys. This SPTA assembly has been designed for samples of about 2 cm³. Three type-S (Pt–10 wt.%Rh/Pt) thermocouples have been employed for the measurement of temperatures, i.e. one in each crucible and one directly at the center of the sample. In order to avoid a chemical reaction between the thermocouple and the sample, the sample thermocouple was coated with a very thin layer of BN.

In order to perform thermal analyses, the assembly was inserted in the furnace chamber of an electrical heat treatment furnace. Before each experimental run, the furnace chamber was closed and evacuated. Finally, a protective
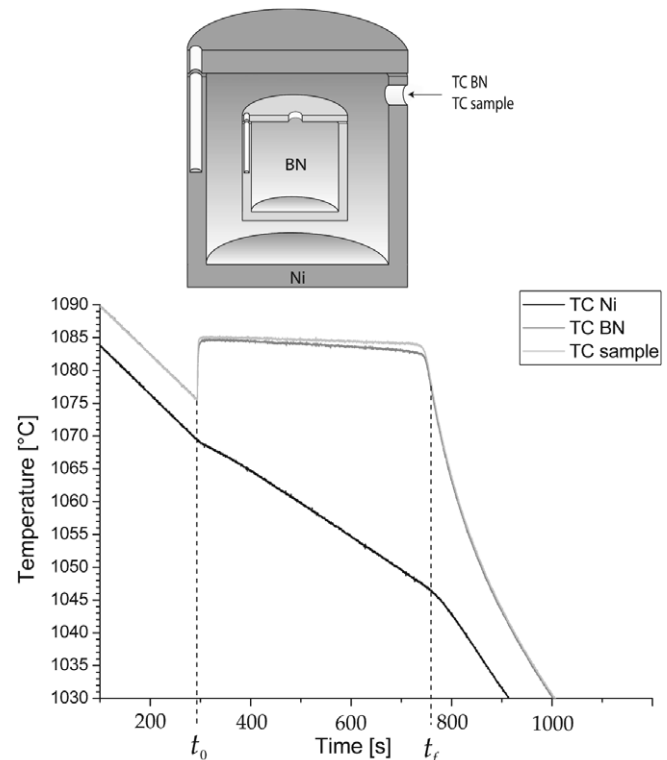

Fig. 1. On top, illustration of the SPTA assembly (the alumina ring used to center the BN crucible is not represented here). Cooling curves measured at the center of the sample (TC sample), in the BN crucible (TC BN) and in the Ni envelope (TC Ni) during a SPTA on a Cu–99.99 wt.%. t_0 and t_f correspond to the start and end of solidification, respectively.

argon flux was allowed to pass through the chamber to avoid oxidation. All thermal analyses have been carried out with the same procedure: after a rapid heating to 1200 °C, the temperature was held for 3 h to ensure a complete remelting of the sample and a uniform temperature through the SPTA assembly. Then, an imposed cooling rate of −5 K min⁻¹ was set until the furnace chamber reached room temperature. Temperatures were recorded every 0.2 s during the calibration procedure and every 0.8 s during thermal analyses of Cu–Sn alloys.

The calibration of the SPTA assembly was performed with two types of experimental runs: one with an empty BN crucible and one with pure Cu–99.99 wt.%, i.e. reference material. Accordingly, temperature-dependent heat capacities C_p (J kg⁻¹ °C⁻¹) have been used: for BN, $C_{p\,BN}(T) = 619.6 + 1.08 T_{BN} - 0.00051 T_{BN}^2$ where T_{BN} is the BN temperature [11]; for pure Cu–99.99 wt.%, $C_{p\,Cu}(T)$ has been deduced from an enthalpy vs. temperature tabulation provided by ThermoCalc™.

Cu–Sn samples were cast in a vacuum induction furnace from appropriate weights of Cu–99.99 wt.% and Sn–99.99 wt.%. In order to fit in the BN crucible, the cast samples were then machined to a cylindrical geometry, i.e. $\phi = 13.8$ mm, $h = 15$ mm, with a 10 mm deep hole drilled at the center for the thermocouple. Finally, the machined samples were thoroughly cleaned with ethanol in an ultrasonic bath to remove all machining waste. After each thermal analysis, the solidified samples were cut in two halves and polished using SiC papers of different grits. For fine polishing, 1 and 0.25 μm diamond-spray particles on soft clothes have been used, followed by a polishing for 1 h on a vibrometer with an alumina colloidal suspension. After polishing, a rapid chemical etching was done to reveal the phases present in the microstructures. For this purpose, all samples were plunged during 5 s in a solution made up of potassium chromate $K_2Cr_2O_7$, sulfuric acid H_2SO_4 and distilled water (solution provided by Wieland-Werke AG [12]).

Three typical cooling curves measured at the center of a Cu–99.99 wt.% sample, in the BN crucible and in the Ni envelope are shown in Fig. 1. The nucleation event followed by a recalescence of nearly 9 K can be clearly observed at the onset of solidification (marked at t_0). The end of solidification is also visible on all curves, even that measured in the Ni envelope. These curves were then used as input for the calculation of the evolution of the solid mass fraction as a function of temperature, $f_s(T)$, according to the heat flow model presented in the following section.

3. Heat flow model

The sample (S), BN crucible (BN) and Ni envelope (Ni) have a mass m_S, m_{BN} and m_{Ni}, respectively. For the sample, the indices 's' and 'l' will be used to specify quantities over the solid and liquid phases, respectively. The heat transfer coefficient between the sample and the crucible is denoted α_1 while that between the crucible and the envelope is α_2,

whereas the corresponding surfaces of heat exchange are written as A_1 and A_2, respectively.

With these definitions, and assuming that the temperature of each medium, i.e. sample (T_S), BN crucible (T_{BN}) and envelope (T_{Ni}), is uniform, the heat balance for the sample is simply given by:

$$m_S \frac{d\langle h_S \rangle}{dt} = -\alpha_1 A_1 (T_S - T_{BN}) \tag{1}$$

where $\langle h_S \rangle$ is the sample specific enthalpy averaged over the solid and liquid phases. Similarly, for the BN crucible:

$$m_{BN} \frac{dh_{BN}}{dt} = \alpha_1 A_1 (T_S - T_{BN}) - \alpha_2 A_2 (T_{BN} - T_{Ni}) \tag{2}$$

where h_{BN} is the specific enthalpy of the BN crucible.

The heat transfer coefficient $\alpha_2(T_{BN}, T_{Ni})$ between the crucible and the envelope is a result of convection of the argon gas and radiation (conduction can be neglected). As the crucible is fully surrounded by the envelope, this coefficient can be approximated as [13]:

$$\begin{aligned} \alpha_2 &= \alpha_2^{conv} + \alpha_2^{rad} \\ &= \alpha_2^{conv} + \sigma_{SB}\epsilon_r(T_{BN}^2 + T_{Ni}^2)(T_{BN} + T_{Ni}) \end{aligned} \tag{3}$$

where α_2^{conv} and α_2^{rad} are the convective and radiative contributions to the heat transfer coefficient $\alpha_2(T_{BN}, T_{Ni})$, respectively. $\sigma_{SB} = 5.67 \times 10^{-8}$ Wm⁻² K⁻⁴ is the Stefan–Boltzmann constant and ϵ_r the relative emissivity of the BN crucible. As $\alpha_2(T_{BN}, T_{Ni})$ does not depend on the stage of solidification of the sample, the product $\alpha_2 A_2$ can be fitted on a calibration made on an empty crucible or with a known reference material (e.g. pure Cu) (see Section 3.2). The other heat transfer coefficient entering into Eqs. (1) and (2) not only depends on the temperatures of the sample and of the crucible, but also on the fraction of solid, i.e. $\alpha_1(T_S, T_{BN}, f_s)$. Indeed, thermal contact, and thus conduction, between the sample and the crucible might be good in the liquid state, but then could decrease upon solidification due to the formation of an air gap (solidification shrinkage). Fortunately, this term can be eliminated by adding Eqs. (1) and (2), thus giving:

$$\begin{aligned} m_S \frac{d\langle h_S \rangle}{dt} &= -m_{BN} \frac{dh_{BN}}{dt} - \alpha_2 A_2 (T_{BN} - T_{Ni}) \\ &= -m_{BN} C_{p\,BN} \frac{dT_{BN}}{dt} - \alpha_2 A_2 (T_{BN} - T_{Ni}) \end{aligned} \tag{4}$$

Therefore, with the three temperatures known from the measurements, the temperature-dependent specific heat of BN, $C_{p\,BN}$, known (see Section 2) and the last right-hand side term of Eq. (4) being fitted from a calibration measurement, the variation of enthalpy of the sample can be deduced.

In order to avoid at this stage the use of a predefined microsegregation model for the calculation of the solid mass fraction f_s from temperature measurements, the concentration over each phase is assumed to be uniform in a first step. Consequently, the sample enthalpy is uniform over the solid and liquid phases and $\langle h_S \rangle$ can be developed as:

$$\langle h_S \rangle = f_s h_{S,s} + (1 - f_s) h_{S,l} \tag{5}$$

The specific enthalpy of the solid phase, $h_{S,s}$, and liquid phase, $h_{S,l}$, can be deduced from a thermodynamic database such as ThermoCalc™. Indeed, as will be detailed in the next section, for every time t during alloy solidification there is a corresponding measured temperature T_S, and, accordingly, equilibrium concentrations in the solid and liquid phases. Consequently, the time-dependent latent heat of fusion $l(t)$ is defined as the difference between $h_{S,l}(t)$ and $h_{S,s}(t)$: $l(t) = h_{S,l}(t) - h_{S,s}(t)$:

$$\frac{d\langle h_S \rangle}{dt} = f_s \frac{dh_{S,s}}{dt} + (1 - f_s) \frac{dh_{S,l}}{dt} - l(t) \frac{df_s}{dt} \tag{6}$$

Obviously, if more than one solid phase solidifies (see Fig. 2), the enthalpy of the corresponding phase must be considered, e.g. α and β in the case of a peritectic reaction.
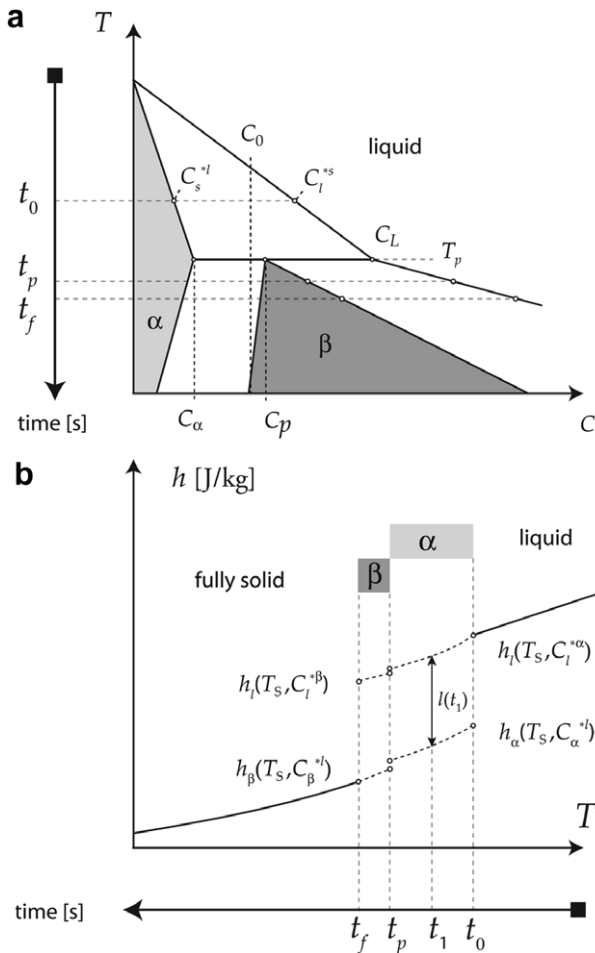

Fig. 2. (a) Schematic peritectic phase diagram with a time scale on the left illustrating the time evolution during a typical SPTA experiment. The solidification of an alloy of composition C_0 in the hypoperitectic range is considered, where t_0 and t_p correspond to the onset of α- and β-phase nucleation, respectively. For each time t there is a corresponding sample temperature and interface concentrations. (b) The coupling with Thermo-Calc™ is shown for a time t_1 during α-phase solidification, where $h_{S,l}(t_1) = h_l(t_1)$ and $h_{S,s}(t_1) = h_\alpha(t_1)$ can be deduced. Simultaneously, the latent heat $l(t_1)$ is obtained.

Since the solid mass fraction $f_s(t)$, or equivalently $f_s(T_S)$, being sought, one gets the following first-order differential equation:

$$f_s \frac{dh_{S,s}}{dt} + (1 - f_s) \frac{dh_{S,l}}{dt} - l(t) \frac{df_s}{dt}$$
$$= -\frac{1}{m_S} \left(m_{BN} C_{p\,BN} \frac{dT_{BN}}{dt} + \alpha_2 A_2 (T_{BN} - T_{Ni}) \right) \tag{7}$$

This equation is solved using a simple pivot iterative scheme, i.e. starting with a known $f_s^v(t)$ at iteration v, the solid mass fraction at iteration $v + 1$ is given by:

$$f_s^{v+1}(t) = \int_{t_0}^t \frac{1}{l(t)} f_s^v \dot{h}_{S,s} dt + \int_{t_0}^t \frac{1}{l(t)} (1 - f_s^v) \dot{h}_{S,l} dt$$
$$+ \frac{m_{BN}}{m_S} \int_{t_0}^t \frac{1}{l(t)} C_{p\,BN} \dot{T}_{BN} dt$$
$$+ \int_{t_0}^t \frac{\alpha_2 A_2}{m_S l(t)} (T_{BN} - T_{Ni}) dt \tag{8}$$

where the notation $\dot{\xi}$ has been used to indicate the time derivative of a quantity $\xi(t)$. In order to determine $f_s^{v+1}(t)$, the integration is made over the observed solidification interval defined by t_0 and t_f: t_0 is the time at which solidification starts. Obviously, it is defined when the sample cooling rate shows a sharp peak, i.e. latent heat is released. As the latent heat release is spread over a finite solidification time in alloys, the end of solidification is more difficult to define. Based on the fact that $df_s/dt \to 0$ at the end of solidification, we have defined t_f as the time corresponding to the highest sample cooling rate in absolute value. Indeed, near the end of solidification, the temperature difference between the sample and the Ni envelope is maximum and so is the heat extraction rate (if $\alpha_2 A_2$ is nearly constant). Accordingly, the absolute value of $\dot{T}_S$ reaches a maximum.

For the solidification of pure metals, the latent heat is constant. Consequently, a simplified relation based on Eq. (8) can be deduced:

$$f_s^{v+1}(t) = \frac{1}{l} \int_{t_0}^t \langle C_{pS} \rangle^v \dot{T}_S dt + \frac{m_{BN}}{m_S l} \int_{t_0}^t C_{p\,BN} \dot{T}_{BN} dt$$
$$+ \int_{t_0}^t \frac{\alpha_2 A_2}{m_S l} (T_{BN} - T_{Ni}) dt \tag{9}$$

where the average specific heat of the sample, $\langle C_{pS} \rangle = f_s C_{pS,s} + (1 - f_s) C_{pS,l}$, has been introduced. Again, a simple pivot iterative scheme is necessary to calculate the solid mass fraction, since $\langle C_{pS} \rangle$ depends on f_s. The specific heat of the solid and liquid phases, $C_{pS,s}$ and $C_{pS,l}$, are taken at temperatures corresponding to the end and start of solidification, respectively.

3.1. Coupling with ThermoCalc™

As shown in the previous section, an iterative scheme is necessary to determine the evolution of the solid mass fraction during the solidification of alloys (Eq. (8)). Indeed, the

enthalpies of the solid and liquid phases are temperature- and composition-dependent. Then, for each iteration v, a coupling with a thermodynamic database for the Cu–Sn peritectic system was performed with the following scheme (Fig. 2): for every time t in the solidification interval there is a corresponding measured sample temperature T_S.

Accordingly, assuming that all interfaces are at equilibrium, solid and liquid concentrations at α-liquid, β-liquid and α–β interfaces are deduced from the Cu–Sn phase diagram. Once these concentrations are known, thermodynamic calculations give the corresponding enthalpies $h_{S,s}(t)$ and $h_{S,l}(t)$ at that time, and thus the latent heat $l(t)$. In Fig. 3, the calculated variation of latent heat with temperature during the solidification of a Cu–21.3 wt.% Sn alloy is represented: during nucleation and growth of the α-phase, the latent heat decreases. At 796 °C, a sharp decrease of the latent heat appears, i.e. transition from α- to β-phase solidification. Then, the latent heat is observed to increase linearly up to the end of solidification.

An important issue should be addressed here: depending on the alloy composition, primary α-phase nucleation and growth may be followed by the peritectic reaction α + liquid → β near the peritectic temperature T_p. In order to make the calculations tractable, we assume in the present study that once the peritectic β-phase has nucleated, only the solidification of the β-phase is taken into account. This is equivalent to neglecting during solidification the partial peritectic transformation of the α-phase into the β-phase, but this transformation is much slower than the solidification of liquid into β.

Before using Eq. (8), $f_s^{v=0}(t)$ is calculated using Eq. (9) with the physical properties of pure Cu for the latent heat and for the heat capacity: extensive calculations have shown that five iterations are sufficient for convergence.

For each iteration, the values $h_{S,s}(t)$, $h_{S,l}(t)$, $l(t)$ and $f_s(t)$ are used in Eq. (8) to determine the solid mass fraction $f_s^{v+1}(t)$ at the next iteration. This is repeated until $|f_s^{v+1}(t) - f_s^v(t)| < 10^{-6}$ $\forall t$. One of the main advantages of SPTA is that the sample temperature is directly measured. Consequently, it is fairly simple to finally determine the alloy solidification path $f_s(t) \equiv f_s(T_S) \equiv f_s(T)$. Moreover, the heat flow model developed in the present work allows the solidification path to be determined directly from temperature measurements, without the use of a predefined microsegregation model. The disadvantage is that it is only valid for binary alloys. For multicomponent systems, a microsegregation model (Lever rule, Scheil–Gulliver or back-diffusion) must be used.

3.2. SPTA calibration

Several experimental runs have been carried out with an empty BN crucible during SPTA calibration. Using Eq. (9), the equivalent heat transfer coefficient $\alpha_2 A_2(T_{BN}, T_{Ni})$ $(W\ K^{-1})$ has been calculated and plotted vs. $(T_{BN}^2 + T_{Ni}^2)(T_{BN} + T_{Ni})$. In agreement with Eq. (3), a linear relationship was found:

$$\alpha_2 A_2 = 0.05 + 1.9 \times 10^{-11}\ (T_{BN}^2 + T_{Ni}^2)(T_{BN} + T_{Ni}) \qquad (10)$$

where the first and second terms on the right-hand side refer to the convective and radiative contributions to the heat transfer coefficient $\alpha_2(T_{BN}, T_{Ni})$, respectively. In order to be consistent with the units in Eq. (3), T_{BN} and T_{Ni} are expressed in K. The same SPTA calibration was done with pure Cu–99.99 wt.% and the two coefficients $\alpha_2 A_2(T_{BN}, T_{Ni})$ obtained with an empty crucible and with pure Cu–99.99 wt.% are shown in Fig. 4. As can be seen, these two coefficients are in good agreement and follow the linear relationship of Eq. (3). Consequently, this equivalent heat transfer coefficient will now be used to solve Eq. (8) for the solidification of Cu–Sn alloys.
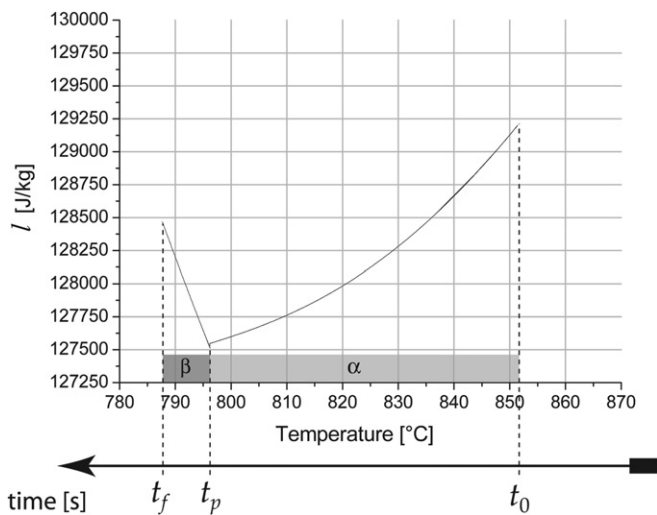

Fig. 3. Calculated temperature evolution of the latent heat during solidification of a Cu–21.3 wt.% Sn alloy (coupling with ThermoCalc™). On the bottom, the time scale during solidification is represented: t_0, t_p and t_f are the times corresponding to the start of solidification, to the peritectic reaction and to the end of solidification, respectively.
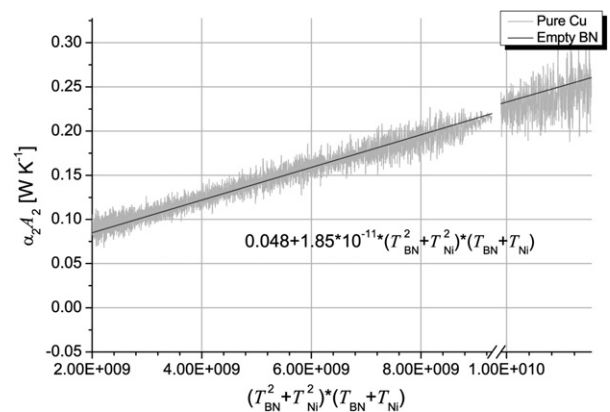

Fig. 4. Equivalent heat transfer coefficient $\alpha_2 A_2$ plotted vs. $(T_{BN}^2 + T_{Ni}^2)(T_{BN} + T_{Ni})$. Dark curve: linear relationship obtained with an empty BN crucible; light grey curve: coefficient calculated with pure Cu–99.99 wt.%.

Using the measured cooling curves of Fig. 1 and the heat flow model previously described, the solid mass fraction of pure Cu has also been calculated using Eq. (9) (Fig. 5). Convergence of $f_s(T)$ was found after five iterations. As already mentioned in Section 2, an important nucleation undercooling of about 9 K followed by a recalescence is revealed. With temperatures recorded every 0.2 s, recalescence has been observed for solid mass fractions between $f_s(T) = 0$ and $f_s(T) = 0.035$. Furthermore, the solidification of Cu is not precisely isothermal: it is spread over about 1 K between the start and the end of solidification. This small temperature decrease of 1 K during solidification is not due to the thermal analysis itself, as it can be observed already on the measured sample cooling curve T_S shown in Fig. 1. So, the possible factors that can explain it are the following: (i) A small temperature gradient within the sample. This is most unlikely because the corresp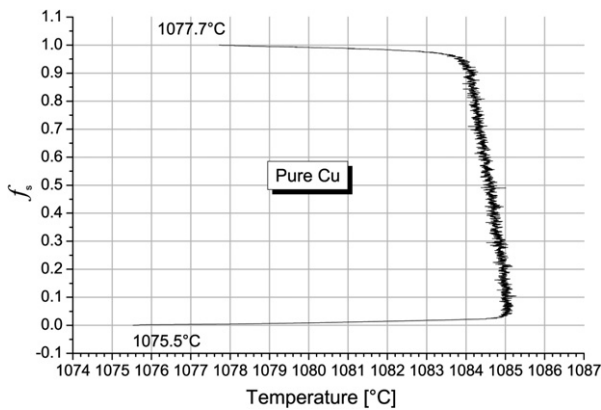onding Biot number is small. (ii) A small temperature difference between the temperature measured by the thermocouple and the sample. This is possible if one considers that solid forms on the thermocouple and that the heat transfer between the thermocouple ceramic and the surroundings increases due to a small contraction. (iii) Rejection of a minute amount of solute. This is the most likely explanation. Taking, for example, phosphorous, a temperature difference of 1 K is obtained with a nominal composition of only 100 ppm assuming the Lever rule. Much less is needed if one considers the segregation associated with the initial and final transients of a nearly planar front. As a matter of fact, 30 ppm of phosphorous has been measured in the cast sample of this copper grade. This last explanation is also supported by the temperature measured just after the recalescence, 1085 °C, which is very close to the one reported in metals handbooks [1]. From $f_s(T) = 0.94$ to the end of solidification, a sudden temperature decrease to 1077.7 °C appeared. Besides the effect mentioned before, this is mainly due to the choice of t_f as being the time corresponding to the maximum $|\dot{T}_S|$. This means that the impingement of the solid parts is more complex and that another criterion should be chosen.

4. Cu–Sn phase diagram

In the literature, numerous Cu–Sn phase diagrams can be found and, most often, these phase diagrams slightly differ. Notably, the reported temperature T_p of the peritectic reaction α + liquid $\rightarrow$ β varies between 795.7 and 798 °C. Until recently, the most widely used and detailed phase diagram is the one reported in Ref. [1] (Fig. 6). In this work, an additional phase diagram for the Cu–Sn peritectic system has been calculated with ThermoCalc™. One of the major advantage of thermodynamic calculations is that
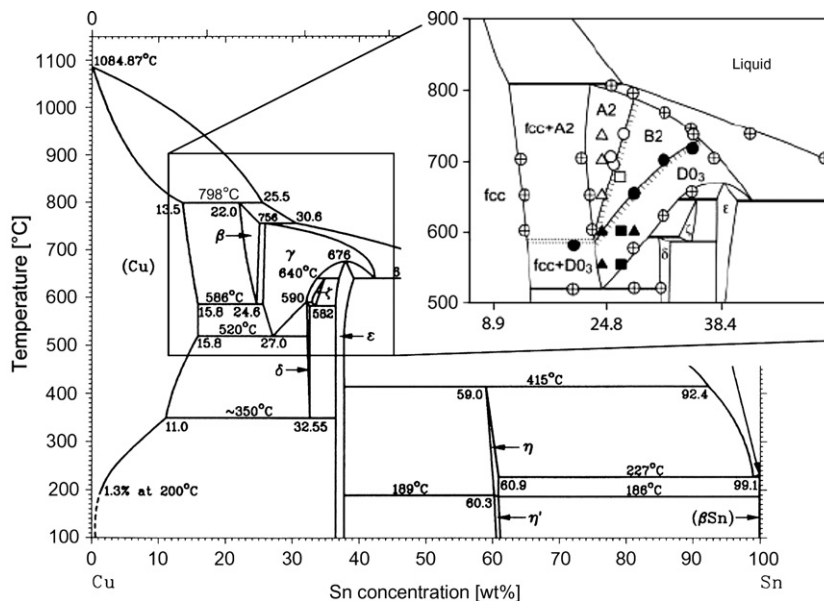

Fig. 5. $f_s(T)$ for pure Cu-99.99 wt%.

Fig. 6. ASM Cu–Sn phase diagram [1]. An enlargement of the β- and γ-phases regions shows the Cu–Sn phase diagram recently reinvestigated by Liu et al. [2].
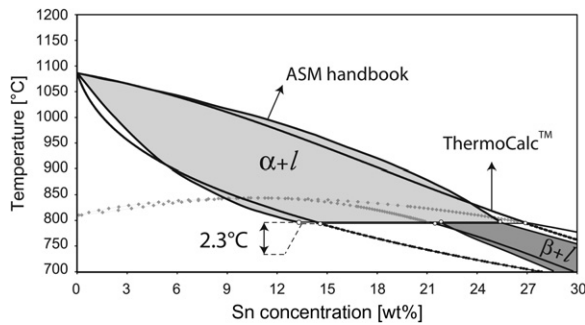
Fig. 7. Comparison of Cu–Sn phase diagrams. Stable solidus and liquidus lines are represented by lines, while small symbols correspond to metastable equilibrium lines (only for the ThermoCalc™ phase diagram).

both stable and metastable equilibrium lines may be obtained for all phases.

In Fig. 7, the Cu-rich portion of the ASM phase diagram [1] represented by shaded areas and the one calculated with ThermoCalc™ are compared for high temperatures: the light grey-shaded area and the dark grey-shaded area correspond to the stable α + liquid and β + liquid two-phase regions, respectively. The continuous curves correspond to the stable equilibrium lines, whereas the metastable equilibrium lines have been represented with small symbols only for the ThermoCalc™ phase diagram.

Let us first consider the α + liquid two-phase region: obviously, this region is quite different between the two phase diagrams. A small difference of 2.3 K is predicted for the peritectic temperature T_p. The concentration difference $C_L(T_p) - C_\alpha(T_p)$ is about the same, but shifted. Both phase diagrams predict that the solidification interval of the α-phase decreases with the tin concentration, a remarkable feature that is important when considering the microstructure competition at very low speed in this system (13.5 wt.% Sn < $C_\alpha(T_p)$ < 14.5 wt.% Sn and 25.5 wt.% Sn < $C_L(T_p)$ < 26.8 wt.% Sn). Surprisingly, the β + liquid two-phase region greatly differs between the two diagrams and the peritectic concentration $C_p \equiv C_\beta$ varies between 21.3 and 22 wt.% Sn.

5. Results

5.1. Cu–14.5 wt.% Sn

Looking at the time derivative of the solid mass fraction during the solidification of a Cu–14.5 wt.% Sn alloy (Fig. 8), two phase transformations can be seen: first, the nucleation and growth of the primary α-phase at 937.8 °C, the peritectic reaction α + liquid → β at 797.5 °C and the solidification end at 791.3 °C. A solid-state phase transformation has also been observed around 515.4 °C. In order to clearly identify this last phase transformation, the solidified microstructure has been investigated: it was composed of pro-peritectic α dendrite arms surrounded by a lamellar structure. Local concentration measurements revealed that this structure was composed
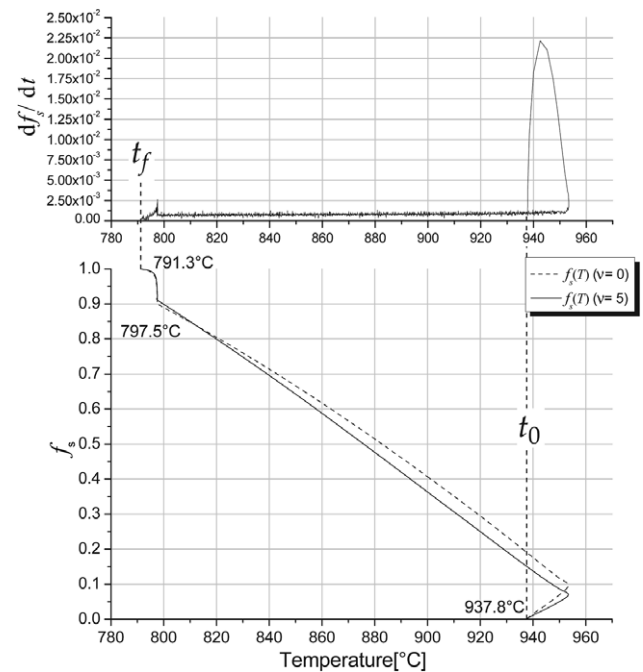

Fig. 8. $f_s(T)$ for a Cu–14.5 wt.% Sn alloy. On top, the time derivative of the solid mass fraction, df_s/dt, is shown ($v = 5$).

of α- and δ-lamellae. Therefore, the observed solid-state phase transformation has been attributed to the eutectoïd $\beta(\gamma) \to \alpha + \delta$ reaction expected to occur at 520 °C (Fig. 6) [14,1].

The solid mass fraction f_s has been calculated using Eq. (8), again using five iterations to obtain convergence. As shown in Fig. 8, f_s is slightly different when considering a constant or variable latent heat during solidification. As for Cu–99.99 wt.%, an important recalescence is observed at the onset of solidification (nearly 15 °C). It corresponds to about 10% of the mass fraction of solid formed during this step. However, one must be careful when considering the start of solidification: as temperatures have been recorded only every 0.8 s, and because of the procedure used for the coupling with ThermoCalc™, recalescence was poorly reproduced. At a solid fraction $f_s(T) = 0.91$, the peritectic reaction, characterized by a small nucleation undercooling, occurs. Indeed, the α-liquid interface acted as nucleation site for the β-phase, thus facilitating its nucleation.

5.2. Cu–21.3 wt.% Sn

As shown in Fig. 7, a Cu–21.3 wt.% Sn alloy is either hypoperitectic or corresponds to the peritectic concentration depending on the considered phase diagram. Based on extensive SPTA made for this alloy composition, four phase transformations have been revealed, the first one occurring around 836 °C (α-phase nucleation). However, this temperature varied between 836 and 861 °C, as a result of variations of the nucleation events. Fortunately, the three other temperatures of phase transformations were

accurately measured: 796 °C for the peritectic reaction and 787.7 °C for the end of solidification. These values are consistent with those determined for the previous alloy. Two solid-state phase transformations have been measured: at 579.2 °C, a very small bump on T_S revealed the presence of a probable second-order reaction. Looking at the recent Cu–Sn phase diagram from Liu et al. [2] (Fig. 6), this reaction has been attributed to the ordering reaction of the β-phase, where it transforms from a disordered A2 structure to an ordered DO3 structure. Finally, another solid-state phase transformation has been observed at 512 °C. As for the Cu–14.5 wt.% Sn alloy, this has been attributed to the eutectoïd $\beta(\gamma) \rightarrow \alpha + \delta$ reaction. Indeed, the solidified microstructure consisted of pro-peritectic α dendrite arms surrounded by a lamellar structure. Again, backscattered electron microscopy and local concentration measurements allowed us to clearly identify the α and δ-phases constituting this lamellar structure (Fig. 9).

The calculated evolution of $f_s(T)$ exhibited slight variations when constant or time-dependent enthalpies are considered (Fig. 10). The recalescence clearly appears, but as already mentioned for the thermal analysis of the Cu–14.5 wt.% Sn sample, it is poorly reproduced in the present study. The peritectic reaction occurred at 796 °C when the mass fraction of the α-phase is $f_s = 0.57$. Again, a negligible nucleation undercooling for the peritectic phase has been observed.

5.3. Cu–26.8 wt.% Sn

According to the ASM Cu–Sn phase diagram [1], a Cu–26.8 wt.% Sn alloy is out of the peritectic range, whereas this composition corresponds to C_L in the phase diagram

Fig. 10. f_s vs. sample temperature T_S for a Cu–21.3 wt% Sn alloy. Dark curve: f_s calculated from Eq. (8). Dark grey curve: f_s calculated from Eq. (9). Dashed black curve: f_s calculated with the microsegregation model (see Section 6). On top, the time derivative of the solid mass fraction, df_s/dt, is shown ($v = 5$).

calculated with ThermoCalc™ (Fig. 7). Thermal analyses on this alloy revealed three phase transformations: the start of solidification appeared at 784.4 °C, about 12 K below the measured peritectic temperature T_p for the Cu–14.5 wt.% Sn and Cu–21.3 wt.% Sn samples. The solidified microstructure consisted of a complex microstructure, where thin precipitates were randomly distributed in a δ-matrix, but no pro-peritectic α-phase was observed. Therefore, the start of solidification was attributed to the nucleation of the peritectic β-phase. Around 772 °C, a slightly exothermic transformation was measured. The solidification ended at 741.8 °C. Finally, a solid-state phase transformation has been observed around 504 °C. But the temperature at which this last transformation occurred showed large variations, i.e. from 487 to 504 °C (see Section 6).

The solid mass fraction $f_s(T)$ has finally been calculated using Eq. (8). In Fig. 11, one sees that the nucleation of the β-phase was followed by a small recalescence. $f_s(T)$ increased monotonically up to the end of solidification, without any sign of second-phase formation. As mentioned above, a slightly exothermic reaction was revealed around 772 °C: but this reaction seemed not to be part of the solidification. If the ASM phase diagram is considered [1] (Fig. 6), the $\beta + \text{liquid} \rightarrow \gamma$ transformation would give a much larger latent heat release and should occur below 756 °C. Therefore, this transformation is most likely attributed to a second-order ordering reaction of the peritectic phase occurring during solidification. These measurements favor the Cu–Sn phase diagram of Liu et al. [2].
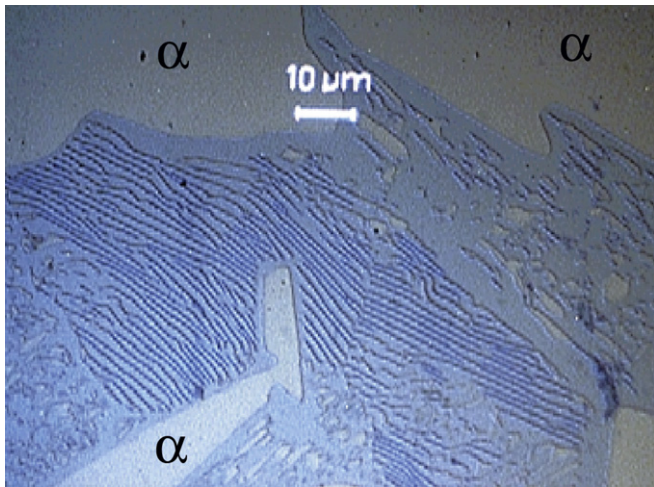

Fig. 9. Cu–21.3 wt.% Sn alloy microstructure after SPTA. A lamellar structure is observed in between pro-peritectic α-phase. Backscattered electron microscopy and concentration measurements showed that this structure consisted of α (dark yellow) and δ-phases (blue). (For interpretation of the references to color in this figure legend, the reader is referred to the web version of this article.)
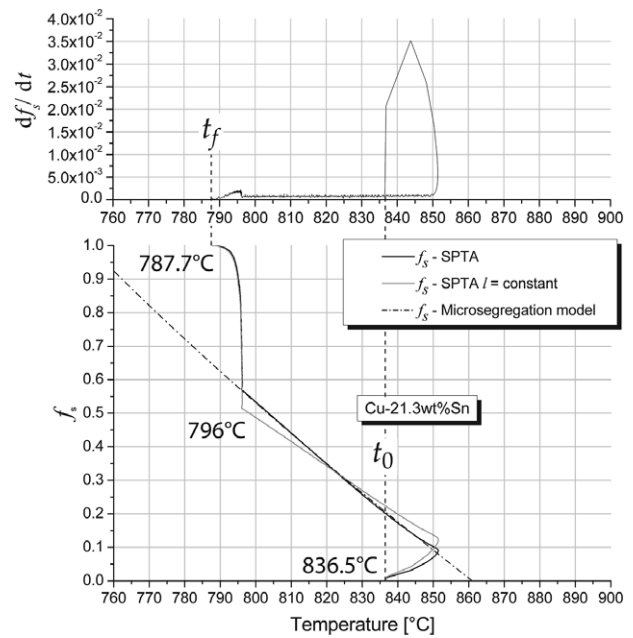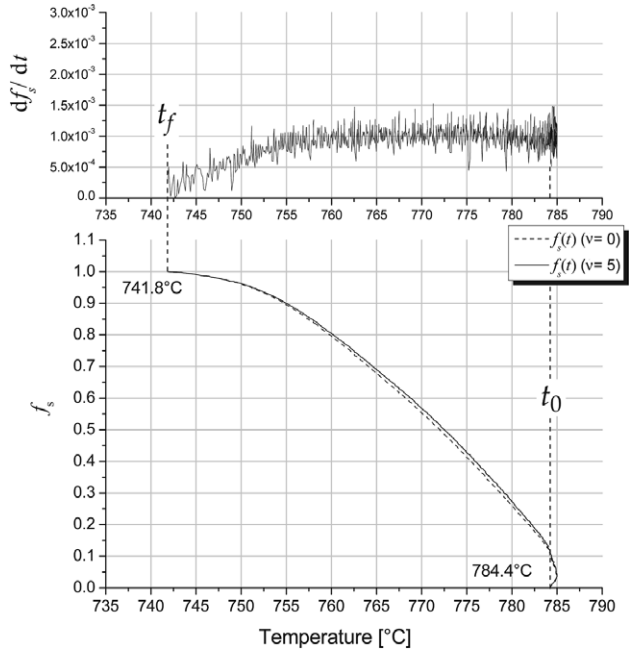
Fig. 11. $f_s(T)$ for a Cu–26.8 wt.% Sn alloy. On top, the time derivative of the solid mass fraction, df_s/dt, is shown ($v = 5$).

6. Discussion

A microsegregation model that includes back-diffusion in the primary α-solid phase has been used to check the accuracy of the developed heat flow model. In the present study, only the α-phase solidification has been modeled. Using the Brody–Flemings microsegregation model [15], one gets:

$$f_s = \frac{1 - \left(\frac{C_l}{C_0}\right)^{\frac{p}{k_\alpha - 1}}}{p} \tag{11}$$

where C_0 and C_l are the nominal and the liquid concentrations, respectively. The parameter $p = 1 - 2k_\alpha Fo_s$ is related to back-diffusion in the solid phase and is therefore a function of the Fourier number, $Fo_s = 4t_F D_s/\lambda_2^2$, where λ_2 represents the secondary dendrite arm spacing, t_F is the solidification time, i.e. $t_F = t_F - t_0$, and D_s corresponds to the diffusion coefficient in the solid.[3]

---

[3] Please note that the same expression is obtained if one uses the volume fraction of solid g_s instead of the mass fraction f_s. In this case, one has:

$$f_s = \frac{\rho_s g_s}{\rho_s g_s + \rho_l(1 - g_s)} \tag{12}$$

where ρ_s and ρ_l are the densities of the solid and liquid, respectively, assumed constant but not equal. But the solute balance has now to consider solidification shrinkage, i.e. the density difference between the solid and liquid phases. Writing $\beta = \left(\frac{\rho_s}{\rho_l} - 1\right)$, one has for a closed volume element:

$$g_s = \frac{1 - \left(\frac{C_l}{C_0}\right)^{\frac{p}{k_\alpha - 1}}}{\beta\left(\frac{C_l}{C_0}\right)^{\frac{p}{k_\alpha - 1}} - \beta + (\beta + 1)p} \tag{13}$$

Table 1
Physical values used in the microsegregation model

Values	Units	Values	Units
$t_F = 1142.7$	s	$Fo_s = 1.411$	–
$\lambda_2 = 39.17$	μm	$D_s = 4.74 \times 10^{-13}$	$m^2\ s^{-1}$

The diffusion coefficient D_s is based on the work from Oikawa and Hosoi [16].

Eq. (11) has been used to model the α-phase solidification of a Cu–21.3 wt.% Sn alloy, assuming a linearized phase diagram near $C_L(T_p)$: $k_\alpha = 0.53$, $m_{l,\alpha} = -11.03$ K wt%$^{-1}$. In Table 1, all parameters used in Eq. (11) are summarized. It should be emphasized that t_F and λ_2 have been measured experimentally.

As can be seen in Fig. 10, the solid mass fractions calculated with Eq. (8) and with the microsegregation model are in perfect agreement. It is interesting to note that, unlike what is usually shown in basic textbooks of solidification [17], the relationship $T(g_s)$ for the solidification of the α-phase is fairly linear (except for the recalescence portion). This is due to the unusual morphology of the α + liquid two-phase region from the Cu–Sn phase diagram. Thus, even if the peritectic reaction and the successive end of solidification have not been modeled, the heat flow model presented here appears to be in good agreement with theoretical models. Furthermore, the SPTA assembly has been well calibrated and the relation with temperature found for the equivalent heat transfer coefficient $\alpha_2 A_2$ is valid for other alloys. For example, the curve $\alpha_2 A_2(T_{BN}, T_{Ni})$ has been used successfully for the thermal analyses of Al–Zn alloys.

Thermal analyses on the Cu–Sn alloys showed that the peritectic reaction α + liquid → β occurred near $T_p = 796 - 797.5\ ^\circ C$. This is in good agreement with the two phase diagrams of Fig. 7. Unfortunately, the recalescence for the peritectic phase is negligible and it is thus very difficult to precisely determine T_p. Furthermore, despite all concentration and temperature analyses made in this work, the three equilibrium concentrations at the peritectic temperature have not been assessed accurately. On the other hand, the solidification of a Cu–26.8 wt.% Sn alloy did not exhibit another peritectic reaction β + liquid → γ at 756 °C, as indicated in most metals handbooks [1]. Consequently, the Cu–Sn phase diagram recently reinvestigated by Liu et al. is certainly the most reliable.

Solid-state phase transformations have also been observed: SPTA on Cu–14.5 wt.% Sn and Cu–21.3 wt.% Sn alloys revealed a phase transformation around 511-515 °C, while thermal analyses on a Cu–26.8 wt.% Sn alloy showed a transformation around 487–504 °C. For the Cu–14.5 wt.% Sn and Cu–21.3 wt.% Sn alloys, the solid-state transformation has been attributed to the decomposition of the peritectic β-phase into a eutectoïd α + δ lamellar structure. Indeed, the liquid concentration at the β-liquid interface has been calculated to vary between 26.5 and 27.6 wt.% Sn during the solidification of the peritectic phase of a Cu–14.5 wt.% Sn alloy, while it varied between

26.8 and 28.4 wt.% Sn for a Cu–21.3 wt.% Sn alloy. Looking at Liu et al.'s phase diagram (Fig. 6), one sees that these composition ranges fall in the hypereutectoïd region ($C_{eut} \approx 24$ wt.% Sn). As a consequence, depending on the local composition in the β-phase, the Sn-rich δ-phase nucleated before the eutectoïd reaction. During the solidification of the peritectic phase for a Cu–26.8 wt.% Sn alloy, the liquid concentration at the β-liquid interface varied between 28.8 and 35.3 wt.% Sn. This fairly large composition range is partly hypereutectoïd and partly located in the δ + ε two-solid phase region. Unfortunately, no concentration measurements could be made due to the very small size of the precipitates. As a consequence, it is still unclear whether some precipitates corresponded to the ε-phase.

Moreover, SPTA on a Cu–21.3 wt.% Sn alloy showed that a probable second-order reaction occurred at 579.2 °C. It has been attributed to an ordering of the peritectic phase, even if no clear experimental observations have been made due to its successive eutectoïd decomposition.

7. Conclusions

In the present study, a SPTA assembly has been built and calibrated. It has been used for thermal analyses of Cu–14.5 wt.% Sn, Cu–21.3 wt.% Sn and Cu–26.8 wt.% Sn alloys. In order to calculate the corresponding evolutions of the solid mass fraction, a new heat flow model has been developed. In this context, a special procedure was determined for a coupling with a Cu–Sn thermodynamic database to deduce the relative evolution of enthalpies during solidification. A close comparison with a microsegregation model that included back-diffusion in the primary α-solid phase allowed us to validate successfully the heat flow model. SPTA on Cu–Sn alloys have shown that the Cu–Sn phase diagram recently reinvestigated in Liu et al.'s review [2] is the most reliable. Obviously, the thermal analysis method developed here can be used for other metals and alloys.

References

[1] American Society for Metals: Metals handbook. Metallography, structures and phase diagrams. 8th ed. Metals Park (OH): ASM International; 1973.
[2] Liu XJ, Wang CP, Ohnuma I, Kainuma R, Ishida K. Metall Mater Trans 2004;35A:1641–53.
[3] Hillert M, Höglund L, Schalin M. Mater Trans 2000;41(8): 1098–103.
[4] Boettinger WJ, Kattner UR. Metall Mater Trans 2002;33A:1779–94.
[5] Wu RI, Perepezko JH. Metall Mater Trans 2000;31A:497–501.
[6] Dong HB, Shin MRM, Kurum EC, Cama H, Hunt JD. Fluid Phase Equilibr 2003;212:199–208.
[7] Dong HB, Hunt JD. J Therm Anal Calorim 2001;64:41–350.
[8] Zou J, Rappaz M. Materials processing in the computer age. Warrendale (PA): TMS; 1991.
[9] Poirier DR, Nandapurkar P. Metall Trans 1988;19A:3057–61.
[10] Dong HB, Shin MRM, Kurum EC, Cama H, Hunt JD. Metall Mater Trans 2003;34A:441–7.
[11] Combat solid boron nitride for molten metal applications. Saint-Gobain Ceramics, Boron Nitride Products; 2003.
[12] Hofmann U, Bögel A, Hölzl H, Kuhn H-A. Prakt Metallogr 2005;42(7):339–64.
[13] Rappaz M, Bellet M, Deville M. Traité des matériaux, Modélisation numérique en science et génie des matériaux, vol. 10. Lausanne: Presses Polytechniques et Universitaires Romandes; 1998.
[14] Cortie MB, Mavrocordatos CE. Metall Mater Trans 1991;22A: 11–8.
[15] D Brody H, Flemings MC. Trans Metall Soc AIME 1966;236:615–24.
[16] Oikawa H, Hosoi A. Scr Mater 1975;9:823–8.
[17] Kurz W, Fisher DJ. Fundamentals of solidification. Zurich: Trans. Tech.; 1998.